



# Geometrical nonlinear analysis by plane quadrilateral element

M. Rezaiee-Pajand\* and M. Yaghoobi

*Department of Civil Engineering, Ferdowsi University of Mashhad, Mashhad, Khorasan Razavi, Iran.*

Received 21 October 2016; received in revised form 23 January 2017; accepted 18 April 2017

## KEYWORDS

Co-rotational method;  
 Geometrical nonlinearity;  
 Strain states;  
 Membrane problem;  
 Quadrilateral element.

**Abstract.** Various co-rotational schemes for solid, shell, bending plate, and beam elements have been proposed so far. Nevertheless, this approach has rarely been utilized for membrane problems. In this paper, a new quadrilateral element will be suggested for solving nonlinear membranes. Simplicity, rapid convergence, and high accuracy of the formulation are the three main characteristics of the presented element. It is worth emphasizing that the recommended element can solve structures with irregular geometry and distorted mesh. This element is insensitive to aspect ratio. In addition, using this element leads to high-accuracy results. Several numerical examples will be tested to prove the high precision of the element in coarse distorted meshes with a large aspect ratio.

© 2018 Sharif University of Technology. All rights reserved.

## 1. Introduction

Extensive researches have been carried out to present efficient elements. The aim has been to find simple elements, which lead to results with engineering accuracy in coarse meshes [1]. Convergence, invariance to coordinate, rank sufficiency, similar accuracy in displacements and strains, insensitivity to geometric distortion, and ability to mix with other elements are the main characteristics of high-performance elements. Additionally, these elements can be extended simply and usefully in solving nonlinear problems [2]. Free formulation aims to directly construct the entries of the stiffness matrix responsible for satisfaction of the patch test. In this procedure, the stiffness matrix is divided into two parts: basic and high order. Bergan et al. studied this kind of methods for a decade [3]. In 1984, by using the results of these works, Bergan and Nygard conducted the free formulation based

on incompatible displacement and individual element test [4,5]. A high-performance finite element for structural mechanics is a simple element that can find the results with engineering accuracy for the coarse meshes. This simple element should have a few degrees of freedom. In 1986, Park and Stanley employed an assumed natural strain formulation to propose high-performance elements [6]. This technique was based on the independent displacement and strain field. A good merit of this strategy was the stiffness matrix that never suffered from rank deficiency. However, it did not respond adequately to the individual element test [7].

It should be noted that combining free formulation with the assumed natural strain formulation leads to the assumed natural deviatoric strain technique. Militello and Felippa have fully explained how to construct an element by employing assumed natural deviatoric strain method [8,9]. By utilizing free parameters, continuous space of elastic functionals is defined. Inserting eigenvalues for free parameters forms the well-known elastic functionals such as potential energy, Hellinger-Reissner, and Hu-Washizu. Utilizing the free formulation and assumed natural strain formulation will make stationary of the parametrized

\*. Corresponding author.  
 E-mail addresses: [mrpajand@yahoo.com](mailto:mrpajand@yahoo.com) (M. Rezaiee-Pajand); [majidyaghoobi@yahoo.com](mailto:majidyaghoobi@yahoo.com) (M. Yaghoobi)

functional. In this way, parametrized algebraic form of the stiffness matrix, called finite element template, can be established [10,11].

The optimization procedure of the finite element template is complicated and requires innovation. Large number of free parameters, index processing, and optimization of the matrix patterns are the main drawbacks of finite element template method. To achieve simplicity and accuracy in analysis of mega structures, researchers try to find high-performance elements with low-order fields. As a result of these attempts, various types of membrane quadrilateral elements have been presented. The structures that have irregular geometry can be easily meshed with the help of four-node elements. By employing strain gradient notation tactic, optimality constraints such as insensitivity to geometric distortion, rotational invariance, satisfying equilibrium equations, and elimination of the parasitic shear error can be included into the formulation of the element [12-15].

To extend these properties into geometrical non-linear problems, co-rotational technique is deployed. Co-rotational scheme is a simple procedure for creating elements suitable for geometric nonlinear analysis. Taking advantage of this strategy provides the possibility of utilizing the linear formulation for nonlinear behavior. Up to now, different co-rotational elements such as solid, shell, bending plate, and beam have been proposed. Nevertheless, this approach has rarely been utilized for membrane problems. Separation of the element movement into two parts, namely, rigid body motion and the one with pure deformation, forms the main idea of the co-rotational tactic. In other words, the fundamental concept of co-rotational description is decomposition of the reference configuration into rigid body and deformational motions. By splitting the body motions into the aforementioned parts, the co-rotation configuration is attained. The Cartesian coordinates, associated with this configuration, move with the element. The pure deformation is measured with respect to these coordinates. In addition, a transformation matrix is required to correlate the base coordinates with the co-rotational coordinates. Most formulations are complex. Hence, it is not easily possible to convert them from linear form to the nonlinear one. One of the well-known complicated formulations was proposed by Felippa [16].

Several researchers have utilized quadrilateral elements for the analyses of membrane problems. Eight-noded serendipity element and nine-noded Lagrangian quadrilateral element have been used for numerous times [17-21]. The number of degrees of freedom in these elements is high. Increasing the number of degrees of freedom intensifies the complexity of the elements. As a result, it leads to extra computational cost, and it adds to the complexity of the nonlinear

analyses. Fortunately, the proposed element has a few degrees of freedom.

In structural nonlinear problems, sensitivity to the geometric distortion leads to considerable errors in results. For achieving appropriate outcome, it is sometimes essential to remesh the body. This process is very expensive. On the other hand, the geometric distortion is inevitable in huge structures with irregular geometry. In this paper, several numerical tests are performed to prove the efficiency of the proposed formulation in the nonlinear analysis. The proposed element has insensitivity to the aspect ratio and geometric distortion. Having these properties in hand increases the accuracy of the obtained results. It should be reminded that only a few benchmark problems related to the nonlinear membrane are available. To overcome this shortage, the authors were forced to include some beam problems in the numerical tests. However, all findings clearly demonstrate that the suggested element is efficient.

## 2. Formulation for linear behavior

Contrary to displacement tactic, Taylor series of the strain functions is deployed in strain gradient notation technique. For two dimensional problems and in  $xy$  plane, three strain functions are existed. Taylor's series expansions of these functions, around the origin of coordinates, have the following form:

$$\begin{aligned}\varepsilon_x(x, y) &= (\varepsilon_x)_o + (\varepsilon_{x,x})_o x + (\varepsilon_{x,y})_o y + (\varepsilon_{x,xx})_o \left(\frac{x^2}{2}\right) \\ &\quad + (\varepsilon_{x,xy})_o (x \cdot y) + (\varepsilon_{x,yy})_o \left(\frac{y^2}{2}\right) + \dots, \\ \varepsilon_y(x, y) &= (\varepsilon_y)_o + (\varepsilon_{y,x})_o x + (\varepsilon_{y,y})_o y + (\varepsilon_{y,xx})_o \left(\frac{x^2}{2}\right) \\ &\quad + (\varepsilon_{y,xy})_o (xy) + (\varepsilon_{y,yy})_o \left(\frac{y^2}{2}\right) + \dots, \\ \gamma_{xy}(x, y) &= (\gamma_{xy})_o + (\gamma_{xy,x})_o x + (\gamma_{xy,y})_o y \\ &\quad + (\gamma_{xy,xx})_o \left(\frac{x^2}{2}\right) + (\gamma_{xy,xy})_o (xy) \\ &\quad + (\gamma_{xy,yy})_o \left(\frac{y^2}{2}\right) + \dots\end{aligned}\quad (1)$$

In this equation,  $(\varepsilon_x)_o$  denotes the magnitude of axial strain  $\varepsilon_x$  in the origin. In addition,  $(\varepsilon_{xx})_o$  and  $(\varepsilon_{xy})_o$  are the rate of  $\varepsilon_x$  variation in  $x$  and  $y$  directions, in the origin's vicinity, respectively. It should be mentioned that the magnitudes of the strain gradient at the origin are named the strain states. In 2D states, three rigid motions are possible. These rigid motions lead to zero

strain states. As a result, the rigid body motions are not considered in Taylor series of the strain field. The displacement field is expressed in terms of strain states when strain gradient notation method is utilized [22]. To achieve this goal, stress-strain relationship of the membrane structures and rotation function of the geometrically linear problem are applied. Using these functions leads to the following results:

$$\varepsilon_x = \frac{\partial u}{\partial x}, \quad \varepsilon_y = \frac{\partial v}{\partial y}, \quad \gamma_{xy} = \frac{\partial u}{\partial y} + \frac{\partial v}{\partial x}, \quad (2)$$

$$r_r = \frac{1}{2} \left( \frac{\partial v}{\partial x} - \frac{\partial u}{\partial y} \right). \quad (3)$$

By calculating the coefficients of the displacement interpolation field in terms of the strain states, the field functions of the element can be written as follows:

$$\begin{cases} u = u_o + (\varepsilon_x)_o x + (\gamma_{xy}/2 - r_r)_o y + (\varepsilon_{x,x})_o x^2/2 \\ \quad + (\varepsilon_{x,y})_o xy + (\gamma_{xy,y} - \varepsilon_{y,x})_o y^2/2 + \dots \\ v = v_o + (\gamma_{xy}/2 + r_r)_o x + (\varepsilon_y)_o y \\ \quad + (\gamma_{xy,x} - \varepsilon_{x,y})_o x^2/2 + (\varepsilon_{y,x})_o xy \\ \quad + (\varepsilon_{y,y})_o y^2/2 + \dots \end{cases} \quad (4)$$

At this stage, the high-performance strain states should be identified. For this purpose, several optimality constraints are employed. To find the optimum bending template, the planar pure bending test is proposed by Felippa [16,23,24]. By deploying planar Euler-Bernoulli beam, Felippa investigated the responses of membrane element’s template for planar bending in  $x$  and  $y$  directions. To achieve this goal, the energy ratios ( $r$ ) are measured. In planar bending in  $x$  and  $y$  directions, the internal energy of the rectangular part ( $b \times a$ ) of this beam about  $x$  and  $y$ , namely,  $U_x^{panel}$  and  $U_y^{panel}$ , can be accurately obtained. The strain energy of the aforementioned part under two bending moments, namely,  $M_x$  and  $M_y$ , is calculated. They are shown by  $U_x^{beam}$  and  $U_y^{beam}$  for bending under  $M_x$  and  $M_y$ , respectively. The flexural energy ratios for the  $x$  and  $y$  directions are calculated as  $r_x = \frac{U_x^{panel}}{U_x^{beam}}$  and  $r_y = \frac{U_y^{panel}}{U_y^{beam}}$ , respectively.

In order to study bending effect in  $x$  direction, a beam shown in Figure 1, with two  $M_x$  bending moments applied to its both ends, is considered. The cross-section of the structure is a rectangle with  $b$  and  $h$

dimensions. Bending moment,  $M(x) = M_x$ , is constant throughout the length of the beam. This causes the following stress fields:

$$\sigma_x = \frac{-M_x y}{I_b}, \quad (I_b = \frac{hb^3}{12}), \quad \sigma_y = \tau_{xy} = 0.$$

It is noticeable that the mentioned relationships of the stress functions are valid for the elastic behavior of the structure. Considering these equations, interior energy accumulated in the part  $a \times b$  of the beam is determined as follows:

$$U_x^{beam} = \frac{6aM_x^2}{Eb^3h}. \quad (5)$$

On the other hand, the strain energy caused by  $M_x$  in the part  $a \times b$  has the following relationship:

$$U_x^{panel} = \frac{1}{2} \mathbf{D}_{bx}^T \mathbf{K} \mathbf{D}_{bx}. \quad (6)$$

In this paper, all matrices are written in the bold script. In the last equations,  $\mathbf{K}$  is the stiffness matrix of the rectangular element and  $\mathbf{D}_{bx}$  is the nodal displacement vector corresponding to the bending moment  $M_x$ . The nodal displacements,  $\mathbf{D}_{bx}$ , should be determined. As they are shown in Figure 1, the stress fields produced by bending moments,  $M_x$ , can be formulated in the following form:

$$\sigma_x = -\frac{12M_x y}{b^3 h}, \quad \sigma_y = 0, \quad \tau_{xy} = 0. \quad (7)$$

After finding the stresses, the strain field can be obtained. Then, displacement function can be found by integrating the strains. The energy ratios in  $x$  direction are calculated as follows:

$$r_x = \frac{U_x^{panel}}{U_x^{beam}}. \quad (8)$$

The proposed element can model bending in any arbitrary direction when  $r_x$  or  $r_y$  equals 1. The element is flexible when  $r$  is greater than 1. On the other hand, it is stiff if  $r < 1$ . If  $r$  equals 1 for each aspect ratio of the aforementioned part, the element is optimum in bending. In the case that  $a \gg b$  and  $r_x \gg 1$ , shear locking may occur in  $x$  direction. The parameters  $a$  and  $b$  are dimensions along the  $x$  and  $y$  directions, respectively. In  $y$  direction, shear locking may happen

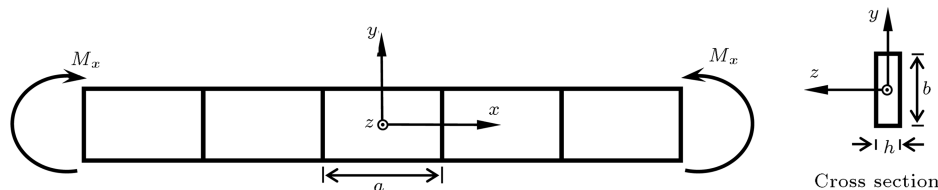


Figure 1. Planar pure bending test in  $x$  direction.

when  $a \ll b$  and  $r_y \gg 1$ . For performing pure bending test in strain gradient notation method, it is necessary to compare real strain states with existing strain states of the beam subjected to pure bending in  $x$  and  $y$  directions [12]. In the case that  $M_x$  is applied, the real strain field includes  $u_o, v_o, (r_r)_o, (\varepsilon_x)_o, (\varepsilon_y)_o, (\varepsilon_{x,y})_o$ , and  $(\varepsilon_{y,y})_o$ . Furthermore,  $u_o, v_o, (r_r)_o, (\varepsilon_x)_o, (\varepsilon_{x,x})_o$ , and  $(\varepsilon_{y,x})_o$  parameters are necessary for the element to correctly model bending behavior under  $M_y$ . No geometry and mesh limits exist in bending tests based on the strain states.

In rotational invariant elements, rotating the coordinate axes does not change any characteristics of the elements. In general, rotating elements can be used to mesh a structure. As a result, it is essential to employ the rotational invariant elements. It is well-known that incomplete interpolation polynomials lead to strain states that are not invariant with the rotation [10]. If the strain field includes all terms with no algebraic order, then the corresponding element will be strain invariant. For instance, selection of the strain field with zero complete order leads to invariant rotational element in a case that the strains are constant.

Appearance of axial strain states in shear strain interpolation polynomial leads to errors, which arise from parasitic shear. These errors make the element stiff [15]. When strain gradient notation is employed to formulate the elements, the parasitic shear errors can be easily removed by omitting the incorrect strain states from shear strain polynomial. Fining the meshes decreases the parasitic shear errors. It should be noted that the parasitic shear errors should be eliminated in coarse meshing to achieve high accuracy. When interpolation functions with complete order are deployed, the parasitic shear errors will not arise [12]. Incomplete field polynomial may lead to incapability of the element to include Poisson’s effect of strain states. Based on the previously investigated optimality constraints, the following strain states are employed for formulation:

$$u_o, v_o, (r_r)_o, (\varepsilon_x)_o, (\varepsilon_y)_o, (\gamma_{xy})_o, (\varepsilon_{x,x})_o, (\varepsilon_{x,y})_o, (\varepsilon_{y,x})_o, (\varepsilon_{y,y})_o, (\gamma_{xy,x})_o, (\gamma_{xy,y})_o. \quad (9)$$

In the isotropic elastic plane stress or strain problems, the equilibrium equations in the element have the following shapes:

$$\begin{cases} \frac{\partial \sigma_x(x,y)}{\partial x} + \frac{\partial \tau_{xy}(x,y)}{\partial y} + F_x(x,y) = 0 \\ \frac{\partial \tau_{xy}(x,y)}{\partial x} + \frac{\partial \sigma_y(x,y)}{\partial y} + F_y(x,y) = 0 \end{cases} \quad (10)$$

where element’s force fields in  $x$  and  $y$  directions of the coordinate systems are shown by  $F_x(x,y)$  and  $F_y(x,y)$ , respectively. They are usually ignored in the equilibrium equations. By employing the stress-strain relationships, Eq. (10) can be expressed in terms

of the strain fields. According to Hooks’ law for isotropic elastic states, the following relations are held for membrane structures:

$$\begin{aligned} \sigma_x &= 2G\varepsilon_x + \lambda(\varepsilon_x + \varepsilon_y), \\ \sigma_y &= 2G\varepsilon_y + \lambda(\varepsilon_x + \varepsilon_y), \\ \tau_{xy} &= G\gamma_{xy}. \end{aligned} \quad (11)$$

For the plane strain and stress states,  $\lambda$  is equal to  $\frac{\nu E}{(1+\nu)(1-2\nu)}$  and  $\frac{\nu E}{(1+\nu)(1-\nu)}$ , respectively. In addition,  $G, \nu$ , and  $E$  denote shear modulus, Poisson[s ratio, and elasticity modulus, respectively. By using Eq. (10), ignoring body forces, and substituting Relations (11) into Eq. (10), the equilibrium equations lead to the next constraints:

$$\begin{cases} (\gamma_{xy,y})_o = -\frac{(2G+\lambda)(\varepsilon_{x,x})_o + \lambda(\varepsilon_{y,x})_o}{G} \\ (\gamma_{xy,x})_o = -\frac{\lambda(\varepsilon_{x,y})_o + (2G+\lambda)(\varepsilon_{y,y})_o}{G} \end{cases} \quad (12)$$

It is obvious that  $(\gamma_{xy,x})_o$  and  $(\gamma_{xy,y})_o$  can be expressed in terms of other strain states. By utilizing these relations, not only the number of unknowns will decrease, but also the efficiency of the element will increase. Herein, the formulations will be carried out based on the remaining 10 strain states. The vector of the strain states has the following shape:

$$\mathbf{q}^T = \left[ u_o \quad v_o \quad (r_r)_o \quad (\varepsilon_x)_o \quad (\varepsilon_y)_o \quad (\gamma_{xy})_o \quad (\varepsilon_{x,x})_o \quad (\varepsilon_{y,x})_o \quad (\varepsilon_{x,y})_o \quad (\varepsilon_{y,y})_o \right]. \quad (13)$$

Accordingly, strain interpolation field can be written in the matrix form as shown in Box I. Moreover, the matrix form of the displacement interpolation field has the shape shown in Box II. By inserting nodal coordinates into Eq. (16), the nodal displacement vector can be obtained as follows:

$$\mathbf{D} = \mathbf{G}_q \cdot \mathbf{q}, \quad (18)$$

$$\mathbf{q} = \mathbf{G}_q^{-1} \cdot \mathbf{D}. \quad (19)$$

By deploying Eqs. (14), (16), and (19), the displacement and strain interpolation fields can be written in terms of the nodal displacements. The obtained fields have the following forms:

$$\mathbf{u} = \mathbf{N}_q \cdot \mathbf{q} = \mathbf{N}_q \cdot (\mathbf{G}_q^{-1} \cdot \mathbf{D}) = \mathbf{N} \cdot \mathbf{D}, \quad (20)$$

$$\mathbf{N} = \mathbf{N}_q \cdot \mathbf{G}_q^{-1}, \quad (21)$$

$$\boldsymbol{\varepsilon} = \mathbf{B}_q \cdot \mathbf{q} = \mathbf{B}_q \cdot (\mathbf{G}_q^{-1} \cdot \mathbf{D}) = \mathbf{B} \cdot \mathbf{D}, \quad (22)$$

$$\mathbf{B} = \mathbf{B}_q \cdot \mathbf{G}_q^{-1}. \quad (23)$$

$$\varepsilon = \mathbf{B}_q \cdot \mathbf{q}, \tag{14}$$

$$\mathbf{B}_q = \begin{bmatrix} 0 & 0 & 0 & 1 & 0 & 0 & x & 0 & y & 0 \\ 0 & 0 & 0 & 0 & 1 & 0 & 0 & x & 0 & y \\ 0 & 0 & 0 & 0 & 0 & 1 & -\frac{(2G+\lambda)}{G}y & -\frac{\lambda}{G}y & -\frac{\lambda}{G}x & -\frac{(2G+\lambda)}{G}x \end{bmatrix}. \tag{15}$$

Box I

$$\mathbf{u} = \mathbf{N}_q \cdot \mathbf{q}, \tag{16}$$

$$\mathbf{N}_q = \begin{bmatrix} 1 & 0 & -y & x & 0 & \frac{y}{2} & \frac{x^2}{2} - \frac{(2G+\lambda)y^2}{2G} & -\frac{(G+\lambda)y^2}{2G} & xy & 0 \\ 0 & 1 & x & 0 & y & \frac{x}{2} & 0 & xy & -\frac{(G+\lambda)x^2}{2G} & \frac{y^2}{2} - \frac{(2G+\lambda)x^2}{2G} \end{bmatrix}. \tag{17}$$

Box II

The stiffness matrix,  $\mathbf{K}$ , can be expressed in terms of elasticity matrix,  $\mathbf{E}$ , by minimizing the strain energy function. The achieved stiffness matrix has the following shape:

$$\mathbf{K} = \int \mathbf{B}^T \cdot \mathbf{E} \cdot \mathbf{B} dV. \tag{24}$$

The formulation needs 10 nodal unknowns. Accordingly, a general five-node quadrilateral element is considered. Therefore, each node has two degrees of freedom. Four nodes are placed at the corners and the fifth one is located at element’s centroid of area. With the help of mathematical operations, the degrees of freedom related to the fifth node can be eliminated. To establish the element formula,  $\mathbf{H}_q$ , is assumed to be the inverse matrix of  $\mathbf{G}_q$ , which can later be divided into two parts. It should be added that the terms with subscripts 1 and 2 are related to the first four nodes and the fifth one, respectively:

$$\mathbf{G}_q^{-1} = \mathbf{H}_q = [\mathbf{H}_{q1} \quad \mathbf{H}_{q2}]. \tag{25}$$

The dimensions of matrices  $\mathbf{H}_{q1}$  and  $\mathbf{H}_{q2}$  are  $10 \times 8$  and  $10 \times 2$ , respectively. Based on Eqs. (21), (23), and (25), the following relationships are obtainable:

$$\mathbf{B} = \mathbf{B}_q \cdot \mathbf{G}_q^{-1} = \mathbf{B}_q \cdot \mathbf{H}_q = [\mathbf{B}_1 \quad \mathbf{B}_2],$$

$$\mathbf{B}_1 = \mathbf{B}_q \cdot \mathbf{H}_{q1}, \quad \mathbf{B}_2 = \mathbf{B}_q \cdot \mathbf{H}_{q2}, \tag{26}$$

$$\mathbf{N} = \mathbf{N}_q \cdot \mathbf{G}_q^{-1} = \mathbf{N}_q \cdot \mathbf{H}_q = [\mathbf{N}_1 \quad \mathbf{N}_2],$$

$$\mathbf{N}_1 = \mathbf{N}_q \cdot \mathbf{H}_{q1}, \quad \mathbf{N}_2 = \mathbf{N}_q \cdot \mathbf{H}_{q2}. \tag{27}$$

Using Eqs. (24) and (26), the subsequent relationship for the stiffness matrix can be achieved:

$$\mathbf{K} = \int \begin{bmatrix} \mathbf{B}_1^T \\ \mathbf{B}_2^T \end{bmatrix} \cdot \mathbf{E} \cdot [\mathbf{B}_1 \quad \mathbf{B}_2] dV = \begin{bmatrix} \mathbf{K}_{11} & \mathbf{K}_{12} \\ \mathbf{K}_{21} & \mathbf{K}_{22} \end{bmatrix}. \tag{28}$$

Therefore, the next well-known governing relation can be formed:

$$\begin{bmatrix} \mathbf{K}_{11} & \mathbf{K}_{12} \\ \mathbf{K}_{21} & \mathbf{K}_{22} \end{bmatrix} \begin{bmatrix} \mathbf{D}_1 \\ \mathbf{D}_2 \end{bmatrix} = \begin{bmatrix} \mathbf{P}_1 \\ \mathbf{P}_2 \end{bmatrix}. \tag{29}$$

In this equation,  $\mathbf{D}_1$  and  $\mathbf{D}_2$  are the nodal displacement vector for the first four nodes and the fifth one, respectively. Omitting the nodal displacement vector for the fifth node, the following equations will be obtained:

$$\mathbf{K}_{11} \cdot \mathbf{D}_1 + \mathbf{K}_{12} \cdot \mathbf{D}_2 = \mathbf{P}_1, \tag{30}$$

$$\mathbf{K}_{21} \cdot \mathbf{D}_1 + \mathbf{K}_{22} \cdot \mathbf{D}_2 = \mathbf{P}_2. \tag{31}$$

Calculating the nodal displacement vector for the fifth node  $\mathbf{D}_2$  and substituting Eq. (31) into Eq. (30) lead to the following result:

$$\mathbf{K}_{11} \cdot \mathbf{D}_1 + \mathbf{K}_{12} \cdot \mathbf{K}_{22}^{-1} \cdot (\mathbf{P}_2 - \mathbf{K}_{21} \cdot \mathbf{D}_1) = \mathbf{P}_1$$

$$(\mathbf{K}_{11} - \mathbf{K}_{12} \cdot \mathbf{K}_{22}^{-1} \cdot \mathbf{K}_{21}) \cdot \mathbf{D}_1 = \mathbf{P}_1 - \mathbf{K}_{12} \cdot \mathbf{K}_{22}^{-1} \cdot \mathbf{P}_2. \tag{32}$$

Finally, the stiffness matrix for the four-node model,  $\bar{\mathbf{K}}$ , is achieved as follows:

$$\bar{\mathbf{K}} = \mathbf{K}_{11} - \mathbf{K}_{12} \cdot \mathbf{K}_{22}^{-1} \cdot \mathbf{K}_{21}. \tag{33}$$

### 3. Co-rotational formulation

To achieve the geometrical stiffness matrix and internal force vector, the co-rotational formulation is employed. In order to obtain the linear stiffness matrix of the

proposed element, the local coordinate system is deployed. It is assumed that the local axes are parallel to the axis of the global coordinate system ( $\bar{x} - \bar{y}$ ). The origin of the local coordinate system is located at element's centroid of area. Rigid translations in  $\bar{x}$  and  $\bar{y}$  directions are demonstrated by  $\bar{u}_o$  and  $\bar{v}_o$ , respectively. Moreover,  $\theta$  denotes rigid rotation. By utilizing these rigid motions, the relationship between the base and the co-rotational coordinates can be written as follows:

$$\begin{bmatrix} u_i \\ v_i \end{bmatrix} = \begin{bmatrix} \cos \theta & \sin \theta \\ -\sin \theta & \cos \theta \end{bmatrix} \begin{bmatrix} \bar{x}_i + \bar{u}_i - \bar{x}_o - \bar{u}_o \\ \bar{y}_i + \bar{v}_i - \bar{y}_o - \bar{v}_o \end{bmatrix} - \begin{bmatrix} x_i \\ y_i \end{bmatrix}, \quad i = 1, 2, 3, 4. \tag{34}$$

In this relation,  $u$  and  $v$  denote displacements in co-rotational frame. By counterclockwise rotating of the local coordinates with the amount of  $\theta$ , the co-rotational coordinates,  $x - y$ , can be obtained. The displacements in the global frame are shown by  $\bar{u}$  and  $\bar{v}$ . Furthermore, the coordinates of use of the centroid are shown by  $\bar{x}_o$  and  $\bar{y}_o$ . To calculate  $\theta$ ,  $\sum_{i=1}^4 (u_i^2 + v_i^2)$  is minimized. Note that  $u_i$  and  $v_i$  denote the nodal displacements of the  $i$ th node in the co-rotational coordinate system [25]. The first derivative of the aforementioned equation with respect to  $\theta$  is set equal to zero. As a result, the following relation is obtained:

$$\tan \theta = \frac{\sum_{i=1}^4 [x_i(\bar{y}_i + \bar{v}_i - \bar{y}_o - \bar{v}_o) - y_i(\bar{x}_i + \bar{u}_i - \bar{x}_o - \bar{u}_o)]}{\sum_{i=1}^4 [x_i(\bar{x}_i + \bar{u}_i - \bar{x}_o - \bar{u}_o) + y_i(\bar{y}_i + \bar{v}_i - \bar{y}_o - \bar{v}_o)]} \tag{35}$$

By solving this equation for  $\theta$ , the extreme points are achieved. These points are  $\theta$  and  $\theta + \pi$ . Among the attained values, the angle which minimizes  $\sum_{i=1}^4 (u_i^2 + v_i^2)$  is chosen. Based on the fact that the virtual work in the co-rotational and global frames is the same, the tangential stiffness matrix and internal forces in the global coordinate system can be calculated by employing a transformation matrix. Note that this matrix relates the co-rotational coordinates to the global one. The governing equations of the element in co-rotational and the global coordinate systems are shown by Eqs. (36) and (37), respectively:

$$\mathbf{F} = \mathbf{K}\mathbf{D}, \tag{36}$$

$$\delta\mathbf{F}_g = \mathbf{K}_g \delta\mathbf{D}_g. \tag{37}$$

In co-rotational coordinate system, force vector, stiffness matrix, and displacement vector are demonstrated

by  $\mathbf{F}$ ,  $\mathbf{K}$ , and  $\mathbf{D}$ , respectively. By employing the above-mentioned transformation matrix, the following result is obtained:

$$\delta\mathbf{D} = \mathbf{T}\delta\mathbf{D}_g. \tag{38}$$

In this equation,  $\mathbf{D}_g$  denotes the displacement vector in the global coordinate system. In addition, the transformation matrix is shown by  $\mathbf{T}$ . To achieve the transformation matrix, the first derivative of Eq. (34) should be calculated as follows:

$$\begin{bmatrix} \delta u_i \\ \delta v_i \end{bmatrix} = \begin{bmatrix} \cos \theta & \sin \theta \\ -\sin \theta & \cos \theta \end{bmatrix} \begin{bmatrix} \delta\bar{u}_i - \delta\bar{u}_o \\ \delta\bar{v}_i - \delta\bar{v}_o \end{bmatrix} + \begin{bmatrix} y_i + v_i \\ x_i + u_i \end{bmatrix} \delta\theta. \tag{39}$$

The equivalent value of can be obtained by deploying Eq. (35):

$$\delta\theta = \sum_{i=1}^4 \frac{1}{\sum_{i=1}^4 [x_i(x_i + u_i) + y_i(y_i + v_i)]} \begin{bmatrix} -y_i & x_i \end{bmatrix} \begin{bmatrix} \cos \theta & \sin \theta \\ -\sin \theta & \cos \theta \end{bmatrix} \begin{bmatrix} \delta\bar{u}_i - \delta\bar{u}_o \\ \delta\bar{v}_i - \delta\bar{v}_o \end{bmatrix}. \tag{40}$$

It is worth emphasizing that pure translational motion causes no rotation. Hence,  $\delta\bar{u}_o$  and  $\delta\bar{v}_o$  can be ignored. By utilizing Eqs. (39) and (40), the transformation matrix can be computed as follows:

$$\mathbf{T} = \mathbf{P}\mathbf{E}^T, \tag{41}$$

$$\mathbf{P} = \mathbf{I} - \mathbf{A}\mathbf{G}, \tag{42}$$

$$\mathbf{A} = \begin{bmatrix} -y_1 - v_1 & x_1 + u_1 & -y_2 - v_2 & x_2 + u_2 \\ -y_3 - v_3 & x_3 + u_3 & -y_4 - v_4 & x_4 + u_4 \end{bmatrix}^T, \tag{43}$$

$$\mathbf{G} = \frac{1}{\sum_{i=1}^4 [x_i(x_i + u_i) + y_i(y_i + v_i)]} \begin{bmatrix} -y_1 & x_1 & -y_2 & x_2 & -y_3 & x_3 & -y_4 & x_4 \end{bmatrix}, \tag{44}$$

$$\mathbf{E} = \text{diag}(\mathbf{R}, \mathbf{R}, \mathbf{R}, \mathbf{R}), \quad \mathbf{R} = \begin{bmatrix} \cos \theta & -\sin \theta \\ \sin \theta & \cos \theta \end{bmatrix}. \tag{45}$$

By using Eqs. (36) to (38), the tangential matrix and internal force vector in the global coordinate system can be expressed in the following form:

$$\mathbf{F}_g = \mathbf{T}^T \mathbf{F}, \tag{46}$$

$$\mathbf{K}_g = \mathbf{T}^T \mathbf{K} \mathbf{T} + \mathbf{K}_h, \quad \mathbf{K}_h = \frac{\partial(\mathbf{T}^T \mathbf{F})}{\partial \mathbf{D}_g}, \tag{47}$$

Employing Eq. (41) and  $\mathbf{A}^T \mathbf{G}^T = \mathbf{I}$  leads to the  $\mathbf{K}_h$

**Table 1.** Deflection of beam subjected to pure bending.

Elements	Regular mesh		Distorted mesh	
	Maximum $u$	Maximum $v$	Maximum $u$	Maximum $v$
ALLMAN	-0.6	1.5	-0.498	1.215
QM6	-0.6	1.5	-0.554	1.384
IB	-0.6	1.5	-0.459	1.124
NSSQ8	-0.6	1.5	-0.6	1.5
Exact [28]	-0.6	1.5	-0.6	1.5

matrix, which has the following shape:

$$\mathbf{K}_h = \delta \mathbf{E} \mathbf{P}^T \mathbf{F} + \mathbf{E} \delta \mathbf{P}^T \mathbf{F} = \mathbf{E} (-\mathbf{H}^T \mathbf{G} - \mathbf{G}^T \mathbf{H} \mathbf{P}) \mathbf{E}^T. \quad (48)$$

It should be added that  $\mathbf{H}$  vector can be obtained as follows:

$$\mathbf{P}^T \mathbf{F} = [a_1 \ a_2 \ a_3 \ a_4 \ a_5 \ a_6 \ a_7 \ a_8]^T, \quad (49)$$

$$\mathbf{H} = [a_2 \ -a_1 \ a_4 \ -a_3 \ a_6 \ -a_5 \ a_8 \ -a_7]^T. \quad (50)$$

#### 4. Geometrical nonlinear numerical tests

To prove the efficiency of the proposed technique in geometrical nonlinear analysis, several numerical tests will be performed. In these examples, coarse mesh with a high aspect ratio is used. In addition, some of the following examples severely suffer from geometric distortion. Some of them have previously been analyzed by employing the robust beam element. In the reference papers, all parameters of the benchmarks are provided without units. All units of the problems are consistent. The elements used throughout this paper are mentioned below:

1. Four-node isoparametric element; Q4 [26];
2. Mixed four-node elements based on the Hu-Washizu functional; HW14-S, HW18-SS [27];
3. Modified non-conforming isoparametric element with internal parameters; QM6 [26];
4. Non-conforming isoparametric element with internal parameters; Q6 [26];
5. Element with internal parameters and formulated by the QACM; AGQ6-I [26];
6. 4-node quadrilateral element with one-point quadrature integration procedure; Qnew [25];
7. Nonlinear four-node quadrilateral element based on strain states; NSSQ8.

##### 4.1. Higher-order patch test

The high-order patch test uses a straight beam under pure bending. The length and width of the beam are 10 and 1, respectively. Regular and distorted

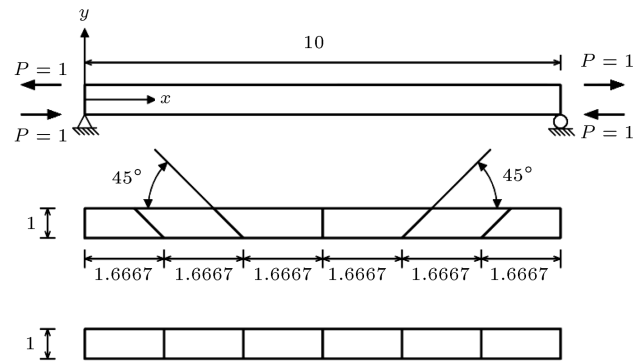


**Figure 2.** Meshing and loading of straight beam subjected to pure bending.

meshes, both consisting of six elements, are used to analyze the structure. Meshing and loading of the structure are shown in Figure 2.  $u$  and  $v$  show the displacements in  $x$  and  $y$  directions. The maximum values of displacements are listed in Table 1. The exact answers are obtained by the beam theory [28]. According to Table 1, NSSQ8 element presents accurate results in both regular and distorted meshes. Moreover, analyzing the response of mesh by one NSSQ8 element is equal to the exact answer. This test demonstrates rapid convergence rate of suggested elements.

##### 4.2. L-shape frame

The geometry of this structure and the applied load pattern are shown in Figure 3(a). One end of the aforementioned frame is completely fixed. At the other

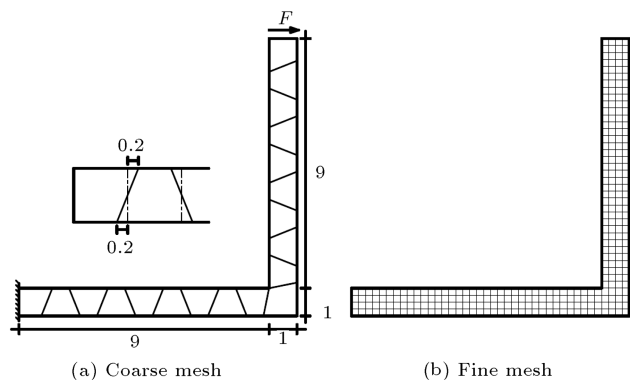


**Figure 3.** Geometry, load pattern, and mesh of the L-shape frame.

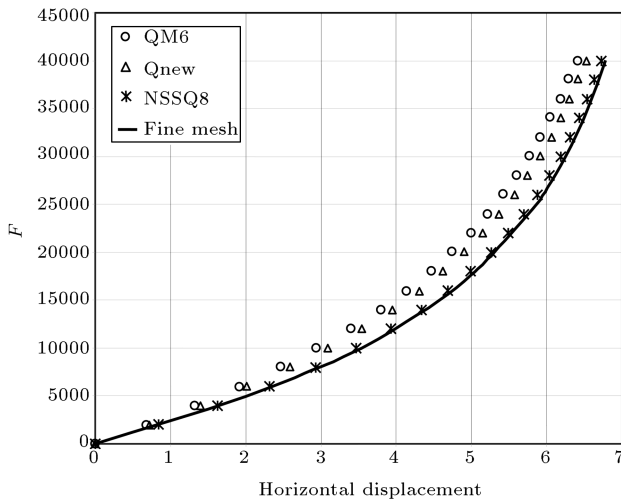


**Figure 4.** Load-displacement diagram of the L-shape frame.

end, a horizontal distributed load with the value of  $F$  is applied. Elasticity modulus and Poisson’s ratio are 30000000 and 0.3, respectively. All units of the problem are consistent. For analyzing this structure, the following fine and coarse meshes are employed. In the coarse mesh, 19 elements are employed and 304 elements are utilized in fine mesh. Figures 3(b) shows the fine mesh.

Previously, QM6 and Qnew elements were utilized for analysis of this frame. For this analysis, nonlinear co-rotational method was employed [25]. The diagrams of the responses of the NSSQ8, QM6, and Qnew overlap when the fine mesh is deployed. It should be reminded that NSSQ8, QM6, and Qnew are used to analyze this frame. Moreover, these elements are applied in both fine and coarse meshes. The obtained results are illustrated in Figure 4. According to the findings for the coarse mesh, the NSSQ8 element leads to more accurate results than QM6 and Qnew elements.

**4.3. Slender cantilever beam under in-plane shear force**

This structure is shown in Figure 5. The length, width, and thickness of the beam are 100, 1, and 1, respectively. Poisson’s ratio and elasticity modulus are 0.3 and 1000000, respectively. Again, all units of the problem are consistent. Note that  $1 \times 100$  meshes are utilized for analysis. In other words, the numbers of elements in  $x$  and  $y$  directions equal 100 and 1, respectively. In this mesh, the aspect

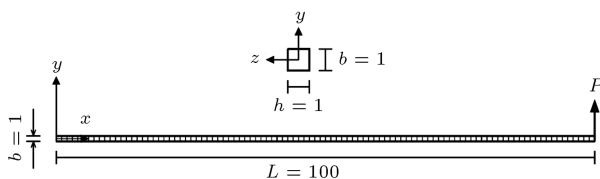


**Figure 5.** Cantilever beam under in-plane shear force.

ratio of the elements is 1. The horizontal and vertical displacements of the free end have previously been calculated. Other researchers have employed HW14-S and HW18-SS elements. They have used  $1 \times 100$  meshes [27]. Furthermore, the responses of this beam are evaluated by applying Timoshenko’s finite rotation beam element [27]. The horizontal and vertical displacements of the aforementioned beam are demonstrated in Figures 6 and 7, respectively.

For the analysis of this structure with  $1 \times 20$  and

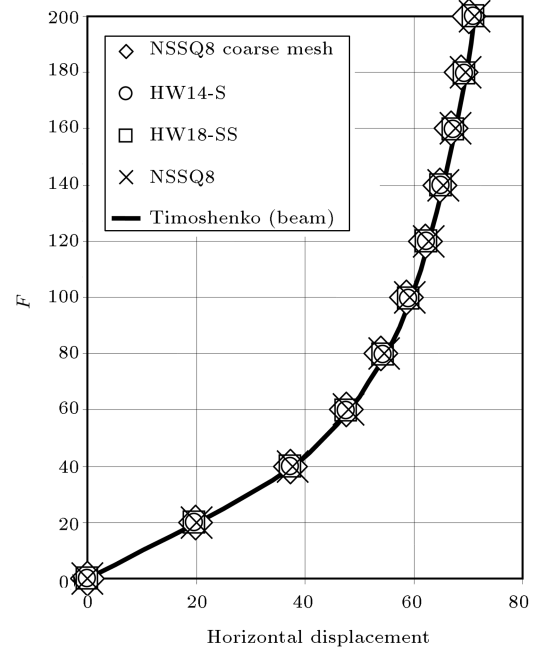


**Figure 6.** Load versus horizontal displacement for the cantilever beam.

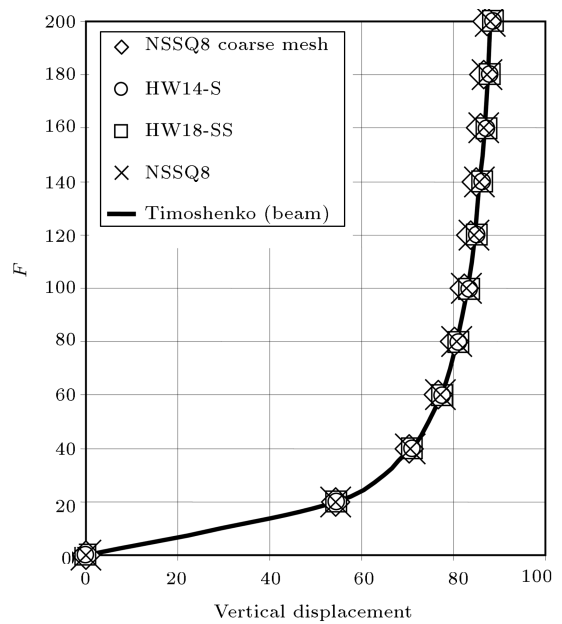


**Figure 7.** Load versus vertical displacement for the cantilever beam.

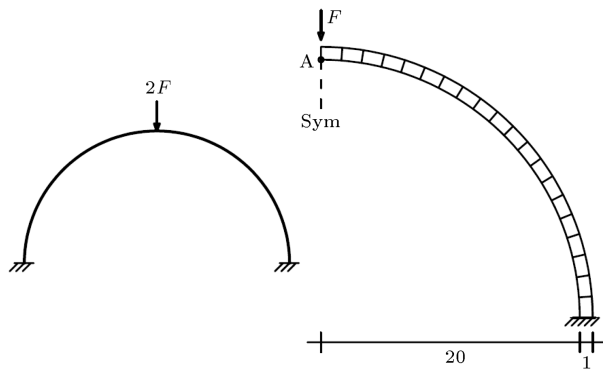


Figure 8. Geometry, load pattern, and mesh of the ring.

$1 \times 100$  meshes, the NSSQ8 element is used. In  $1 \times 20$  meshes, the aspect ratio of elements equals 4. The results obtained by utilizing the NSSQ8 element with  $1 \times 20$  and  $1 \times 100$  meshes are fairly similar to the outcomes of the analysis by employing Timeshenko's finite rotation beam element. Furthermore, it is obvious that the authors' solutions are analogous to the responses of HW14-S and HW18-SS elements.

4.4. Slender ring

In this section, a semicircle ring will be analyzed. Both ends of this ring are fixed. A concentrated load with the value of  $2F$  is applied to the ring. The aforementioned load and the geometry of the ring are illustrated in Figure 8. Due to the symmetry of the structure, only half of it is assessed. Thickness, elasticity modulus, and Poisson's modulus are  $1/\sqrt{12}$ , 2000, and 0, respectively. As before, consistent units are utilized. To analyze this structure, both coarse and fine meshes are deployed. The fine and coarse meshes include  $4 \times 80$  and  $1 \times 20$  meshes, respectively. Figure 8 demonstrates the coarse mesh.

For fine and coarse meshes, the responses of QM6 and Qnew elements have previously been computed by using the geometrical nonlinear co-rotational method [25]. In fine mesh, the responses obtained from employing NSSQ8, QM6, and Qnew are totally similar. Based on Figure 9, it is obvious that using these elements in coarse meshing leads to negligible errors.

4.5. Cantilever beam subjected to shear force at its free end

A cantilever beam is shown in Figure 10. The length and width of this structure are 10 and 0.1478, respectively. In addition, the thickness of this beam equals 0.1. The elasticity modulus and Poisson's ratio are 100000000 and 0, respectively. A shear force with the value of 269.35 is applied to the free end. As before, consistent units are utilized. For analyzing this structure, two coarse meshes are employed. These meshes include  $1 \times 10$  and  $1 \times 20$  elements, respectively. The aspect ratios of these meshes are

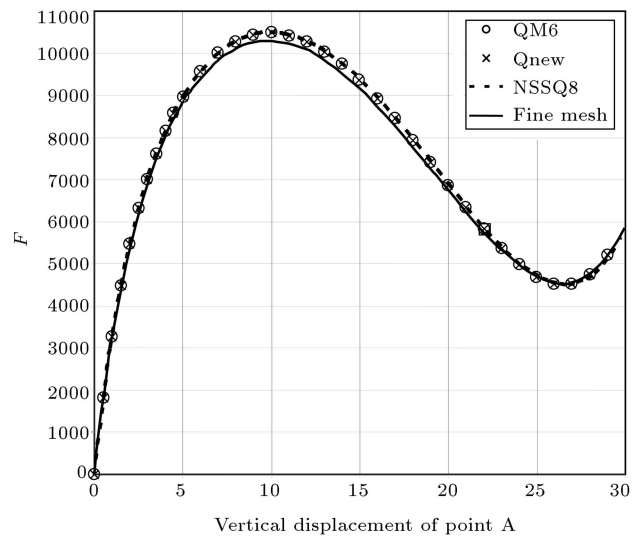


Figure 9. Vertical displacement of the ring at point A.

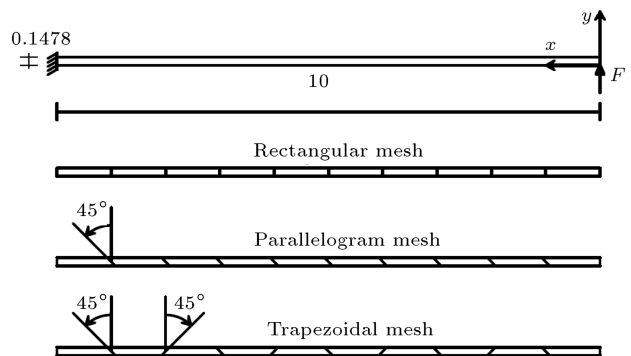


Figure 10. Geometry, load pattern, and mesh of the cantilever beam.

6.8 and 3.4, respectively. Hence, this numerical test investigates the capability of the elements in meshes with a high aspect ratio. Rectangular, parallelogram-shape, and trapezoidal meshes, which include  $1 \times 10$  and  $1 \times 20$  meshes, are deployed to assess the sensitivity of the elements to the geometric distortion. These meshes are illustrated in Figure 10. For each of these structures, the responses of the Q4, Q6, QM6, and AGQ6-I elements have previously been calculated by using the complete Lagrangian geometrical nonlinear technique [26]. These results are presented in Table 2. Furthermore, the responses obtained from geometrical nonlinear co-rotational analysis by utilizing NSSQ8 are given in Table 2. Based on this table, it is obvious that NSSQ8 and AGQ6-I are insensitive to the geometric distortion. Employing Q4, Q6, and QM6 elements in parallelogram-shape and trapezoidal meshes leads to considerable errors. In Table 2,  $u$  and  $v$  denote displacements in  $x$  and  $y$  directions, respectively.

4.6. Beam under eccentric axial load

Figure 11 demonstrates the geometry of the beam structure. The elasticity modulus and the thickness

**Table 2.** Displacements of the cantilever beam.

Elements	Regular		Parallelogram		Trapezoidal	
	1 × 10	1 × 20	1 × 10	1 × 20	1 × 10	1 × 20
Q4	0.1131, 1.444	1.069, 4.166	0.01616, 0.6049	0.1651, 1.748	0.006383, 0.4174	0.06272, 1.129
Q6	5.149, 7.883	5.511, 8.152	3.995, 6.847	5.136, 7.794	0.05401, 1.080	0.3698, 2.630
QM6	5.149, 7.883	5.511, 8.152	3.924, 6.769	5.079, 7.741	0.01731, 0.6498	0.1107, 1.501
AGQ6-I	5.149, 7.883	5.511, 8.152	4.850, 7.736	5.471, 8.137	5.142, 7.859	5.543, 8.171
NSSQ8	5.158, 7.894	5.440, 8.141	5.167, 7.910	5.454, 8.157	5.135, 7.878	5.451, 8.149
Reference [26]			<b>5.546, 8.185</b>			

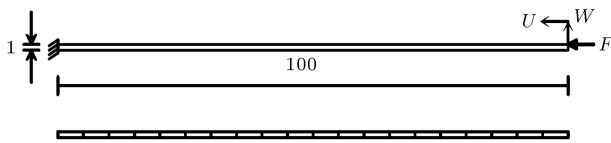


**Figure 11.** Geometry, load pattern, and mesh of the beam.

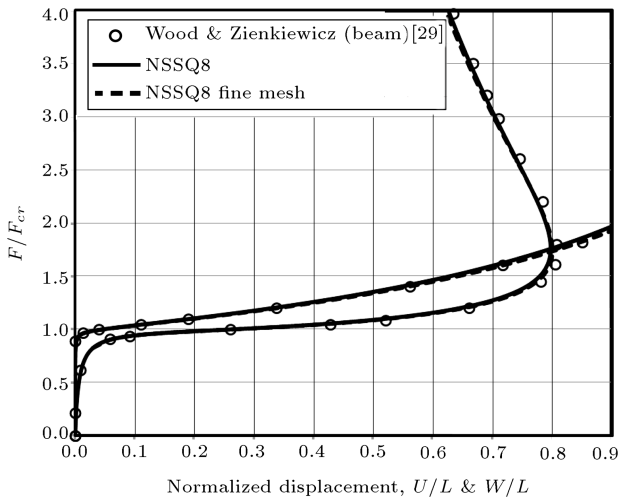


**Figure 12.** Load-displacement curve of the cantilever beam.

of the cantilever beam are 12 and 1, respectively. In solving this problem, consistent units are utilized. Previously, beam elements have been employed to analyze this structure [29]. Herein, this cantilever beam is solved with the NSSQ8 membrane element using  $1 \times 20$  meshes. The diagrams of the aforementioned beam displacements are shown in Figure 12. In this figure, the vertical axis illustrates  $F/F_{cr}$ . In this problem,  $F_{cr} = 0.000247$ . The positive directions of the displacements are demonstrated in Figure 11. In the  $1 \times 20$  mesh, the numbers of elements in the horizontal and vertical directions are 20 and 1, respectively. In this mesh, the aspect ratio of the membrane elements equals 5. To investigate the efficiency of the proposed element, a coarse mesh with a high aspect ratio will be utilized. Based on Figure 12, it is obvious that using the NSSQ8 membrane element in  $1 \times 20$  mesh leads to the results compatible with

the obtained ones from employing the beam elements. For comparison, a fine mesh for the beam, with  $1 \times 100$  meshes, is analyzed by NSSQ8 membrane element.

**4.7. Shallow arch subjected to concentrated load**

The shallow arch structure is demonstrated in Figure 13. It is assumed that the elasticity modulus of the structure is 2000. The cross-sectional area of the arch is equal to 1. Furthermore, the moment of inertia is 1. Yang and Kuo [30,31] analyzed this structure by deploying beam elements. They used a mesh which included 26 elements. To attain this mesh, the arch was divided into 25 sections. Afterwards, the middle element was separated into two sections to gain a new node. This node was placed at the middle of the arch, and the concentrated load was applied to it. To satisfy the support conditions, two rows of elements should be used in the mesh. The demonstrated mesh in Figure 13 is utilized for analysis of this structure by deploying the membrane quadrilateral elements. The aspect ratio of this mesh is equal to 2.3. To utilize the membrane element, the rectangular cross sectional dimensions are presumed to be  $\sqrt{12} \times (1/\sqrt{12})$ . The dimensions of the cross-section are calculated based on the given moment of inertia and cross-sectional area. As a result, the thickness of the structure equals  $(1/\sqrt{12})$ . As before, consistent units are utilized.

In this numerical test, two load cases are applied. For the perfect loading case, it is assumed that the load is applied precisely to the middle node. For the imperfect loading case, it is presumed that the load is applied to the node nearest to the middle node. For analysis of the arch, NSSQ8 is used. The obtained results are shown in Figures 14 and 15. In these figures,

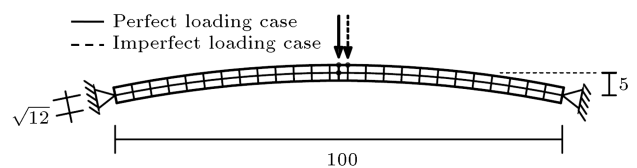


**Figure 13.** Geometry, mesh, and load pattern of the shallow arch.

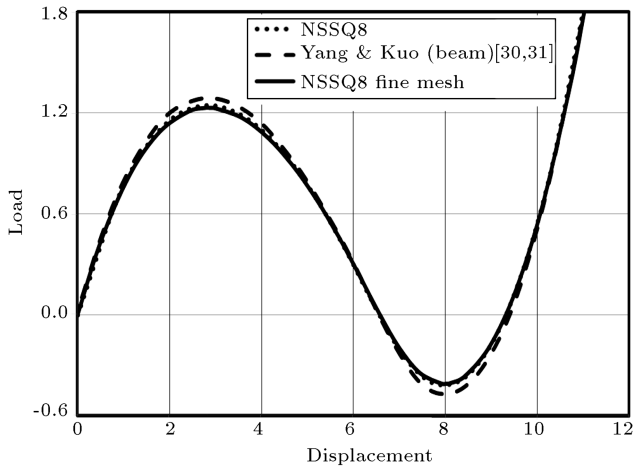


Figure 14. Load-displacement curve in the perfect loading case.

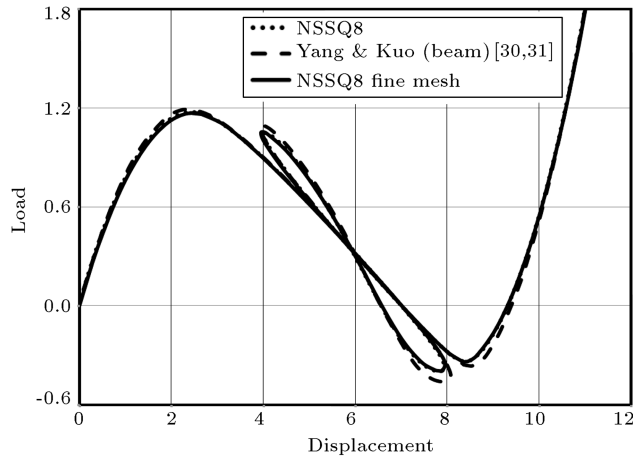


Figure 15. Load-displacement curve in the imperfect loading case.

the displacements of point A, for both mentioned cases, are demonstrated; for comparison, the results found by Yang and Kuo are illustrated [30,31]. High aspect ratio of the mesh and curved geometry of the structure cause some errors. It should be reminded that straight elements are deployed to model the arch. The outcomes are compared with the results of fine mesh. There are 116 NSSQ8 membrane elements in the fine mesh ( $25 \times 8$ ).

4.8. Simply supported semicircle arch

Figure 16 shows the semicircle arch, which is subjected to the concentrated load. Elasticity modulus, moment of inertia, and cross-sectional area of this structure are 2000, 1, and 1, respectively. Based on the cross-sectional area and moment of inertia, it is assumed that the cross section is a  $\sqrt{12} \times (1/\sqrt{12})$  rectangular. For analyzing this structure, the quadrilateral membrane elements are employed. The thickness of the structure is  $(1/\sqrt{12})$ . For this problem, consistent units are utilized. Yang and Kuo [30,31] analyzed this structure

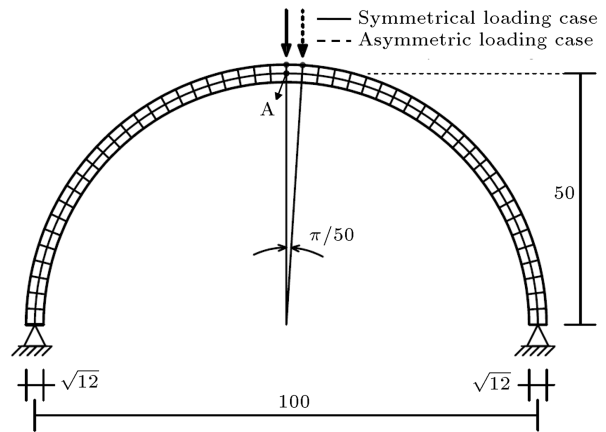


Figure 16. Geometry, mesh, and load pattern of the simply supported semicircle ring.

by deploying 26 beam elements. They divided the structure into 25 equal parts. Afterwards, the middle part was separated into two sections.

Two load cases are employed, which are asymmetric loading and symmetrical load case. In the symmetrical load case, a concentrated load is applied to the middle node. In the asymmetric load case, the concentrated load is applied to the nearest node of the middle one, as it is shown in Figure 16. Herein, two rows of quadrilateral elements are employed to satisfy the support conditions. On the other hand, the  $2 \times 50$  meshes are constructed by dividing the semicircle arch into 50 parts. In this meshing, the aspect ratio is 1.8. Note that straight elements are deployed in modeling of this structure. In fact, curved geometry of the structure leads to errors. The displacements of node A are shown in Figures 17 and 18 under the aforementioned load cases. Under symmetrical load case, the responses of the NSSQ8 element and beam elements are similar. However, the outcomes are fairly the same when the asymmetric load case is applied. For comparison, a fine mesh, containing  $2 \times 100$  NSSQ8 membrane elements, is utilized.

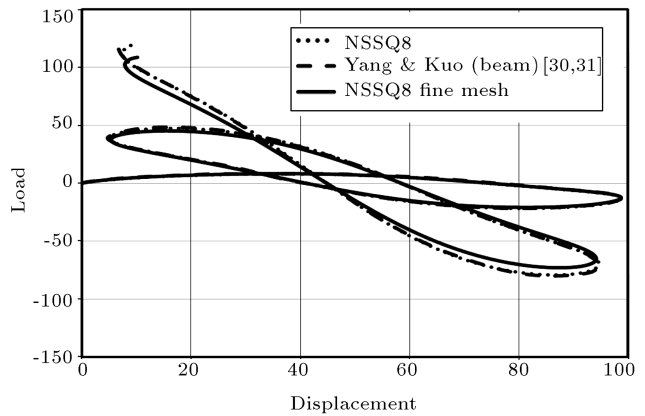
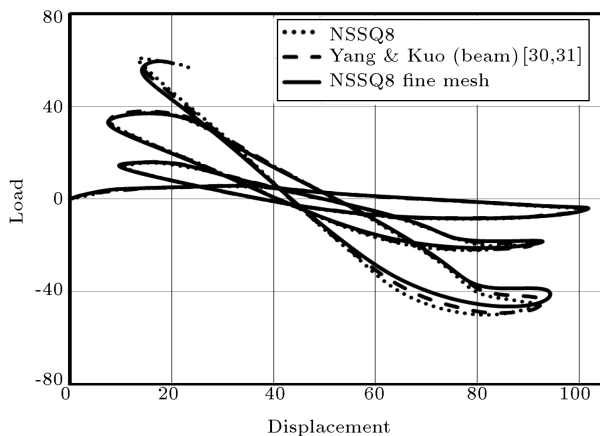


Figure 17. Load-displacement curve of the ring under symmetric load.



**Figure 18.** Load-displacement curve of the ring under asymmetric load.

## 5. Conclusion

By using co-rotational method, the formulation of the suggested element was transformed from linear space into the nonlinear one. In this study, the equilibrium equations of the new quadrilateral membrane element were satisfied. To enhance the ability, several optimality constraints were included. Insensitivity to the coordinates and aspect ratios were the two valuable properties of the presented elements. Moreover, this element did not suffer from the parasitic shear error. Furthermore, the formulation was insensitive to the geometric distortion. In the geometrical nonlinear analysis, all findings showed the insensitivity of the element to aspect ratio and mesh distortion. It was clearly demonstrated that utilizing the proposed element led only to slight errors in the coarse meshes.

## References

1. Felippa, C.A. and Militello, C. "Developments in variational methods for high performance plate and shell elements", In *Analytical and Computational Models for Shells*, CED **3**, Ed. by A.K. Noor, T. Belytschko and J.C. Simo, pp. 191-216, ASME, New York (1989).
2. Felippa, C.A. "A survey of parametrized variational principles and applications to computational mechanics", Invited Chapter in *Science and Perspectives in Mechanics*, Ed. by B. Nayroles, J. Etay and D. Renouard, pp. 1-42, ENS Grenoble, Grenoble, France (1994), Expanded version in *Computer Methods in Applied Mechanics and Engineering*, **113**, pp. 109-139 (1994).
3. Bergan, P.G. and Hanssen, L. "A new approach for deriving 'good' finite elements", In *the Mathematics of Finite Elements and Applications*, Ed. By J.R. Whiteman, **2**, pp. 483-497, Academic Press, London (1975).
4. Felippa, C.A. "The extended free formulation of finite elements in linear elasticity", *Journal of Applied Mechanics*, **56**(3), pp. 609-616 (1989).
5. Bergan, P.G. and Nygard, M.K. "Finite elements with increased freedom in choosing shape functions", *International Journal for Numerical Methods in Engineering*, **20**, pp. 643-664 (1984).
6. Park, K.C. and Stanley, G.M. "A curved C0 shell element based on assumed natural-coordinate strains", *Journal of Applied Mechanics*, **53**, pp. 278-290 (1986).
7. Militello, C. and Felippa, C.A. "A variational justification of the assumed natural strain formulation of finite elements: I. Variational principles", *Computers and Structures*, **34**, pp. 431-438 (1990).
8. Militello, C. and Felippa, C.A. "The first ANDES elements: 9-DOF plate bending triangles", *Computer Methods in Applied Mechanics and Engineering*, **93**, pp. 217-246 (1991).
9. Felippa, C.A. and Militello, C. "Membrane triangles with corner drilling freedoms II. The ANDES element", *Finite Elements Analysis and Design*, **12**, pp. 189-201 (1992).
10. Felippa, C.A. and Militello, C. "The variational formulation of high performance finite elements: parametrized variational principles", *Computers and Structures*, **36**, pp. 1-11 (1990).
11. Felippa, C.A. "Recent advances in finite element templates", Chapter 4, In *Computational Mechanics for the Twenty-First Century*, Ed. by B.H.V. Topping, pp. 71-98, Saxe-Coburn Publications, Edinburgh (2000).
12. Rezaiee-Pajand, M. and Yaghoobi, M. "Formulating an effective generalized four-sided element", *European Journal of Mechanics A/Solids*, **36**, pp. 141-155 (2012).
13. Rezaiee-Pajand, M. and Yaghoobi, M. "A free of parasitic shear strain formulation for plane element", *Research in Civil and Environmental Engineering*, **1**, pp. 1-27 (2013).
14. Rezaiee-Pajand, M. and Yaghoobi, M. "A robust triangular membrane element", *Latin American Journal of Solid and Structures*, **11**, pp. 2648-2671 (2014).
15. Rezaiee-Pajand, M. and Yaghoobi, M. "Two new quadrilateral elements based on strain states", *Civil Engineering Infrastructures Journal*, **48**, pp. 133-156 (2014).
16. Felippa, C.A. "Supernatural QUAD4: A template formulation", *Comput. Methods Appl. Mech. Engrg.*, **195**, pp. 5316-5342 (2006).
17. Grover, N., Singh, B.N., and Maiti, D.K. "Analytical and finite element modeling of laminated composite and sandwich plates: An assessment of a new shear deformation theory for free vibration response", *International Journal of Mechanical Sciences*, **67**, pp. 89-99 (2013).
18. Mehar, K. and Panda, S.K. "Geometrical nonlinear free vibration analysis of FG-CNT reinforced composite flat panel under uniform thermal field", *Composite Structures*, **143**, pp. 336-346 (2016).

19. Hari Kishore, M.D.V., Singh, B.N., and Pandit, M.K. “Nonlinear static analysis of smart laminated composite plate”, *Aerospace Science and Technology*, **15**, pp. 224-235 (2011).
20. Mehar, K. and Panda, S.K. “Numerical investigation of nonlinear thermomechanical deflection of functionally graded CNT reinforced doubly curved composite shell panel under different mechanical loads”, *Composite Structures*, **161**, pp. 287-298 (2017).
21. Mehar, K. and Panda, S.K. “Thermoelastic analysis of FG-CNT reinforced shear deformable composite plate under various loadings”, *International Journal of Computational Methods*, **14**(1), p. 1750019 (22 pages) (2017).
22. Dow, J.O., *A Unified Approach to the Finite Element Method and Error Analysis Procedures*, Academic Press (1999).
23. Felippa, C.A. “A template tutorial”, K.M. Mathisen, T. Kvamsdal and K.M. Okstad, Eds., *Computational Mechanics: Theory and Practice*, pp. 29-68, CIMNE, Barcelona (2004).
24. Felippa, C.A. “A study of optimal membrane triangles with drilling freedoms”, *Comput. Methods Appl. Mech. Engrg.*, **192**, pp. 2125-2168 (2003).
25. Battini, J.M. “A non-linear corotational 4-node plane element”, *Mechanics Research Communications*, **35**, pp. 408-413 (2008).
26. Du, Y. and Cen, S. “Geometrically nonlinear analysis with a 4-node membrane element formulated by the quadrilateral area coordinate method”, *Finite Elements in Analysis and Design*, **44**, pp. 427-438 (2008).
27. Wisniewski, K. and Turska, E. “Improved 4-node Hu-Washizu elements based on skew coordinates”, *Computers and Structures*, **87**, pp. 407-424 (2009).
28. Choi, N., Choo, Y.S., and Lee, B.C. “A hybrid Trefftz plane elasticity element with drilling degrees of freedom”, *Comput. Methods Appl. Mech. Engrg.*, **195**, pp. 4095-4105 (2006).
29. Kien, N.D. “A Timoshenko beam element for large displacement analysis of planar beam and frames”, *International Journal of Structural Stability and Dynamics*, **12**(6), p. 1250048 (9 pages) (2012).
30. Yau, J.D. and Yang, Y.B. “Geometrically nonlinear analysis of planar circular arches based on rigid element concept-A structural approach”, *Engineering Structures*, **30**, pp. 955-964 (2008).
31. Yang, Y.B. and Kuo, S.R., *Theory and Analysis of Nonlinear Framed Structures*, Singapore, Prentice Hall (1994).

### Biographies

**Mohammad Rezaiee-Pajand** received his PhD degree in Structural Engineering from University of Pittsburgh, Pittsburgh, PA, USA. He is currently a Professor at Ferdowsi University of Mashhad (FUM), Mashhad, Iran. His research interests are nonlinear analysis, finite element method, structural optimization, and numerical techniques.

**Majid Yaghoobi** was born in 1985 in Mashhad, Iran. After graduation from the Department of Civil Engineering at University of Mazandaran in 2008, he continued his studies on Structures at Ferdowsi University of Mashhad and received his MS and PhD degrees in 2010 and 2014, respectively. Then, he joined the Torbat Heydarieh University, where he is presently Assistant Professor of Structural Engineering. His research interests include nonlinear finite element formulations.